JOURNAL OF SOLID STATE CHEMISTRY 104, 308–318 (1993)

Structural Characterization of Ge–S and GeS_2–Ag_2S Glassy Range by Sulfur *K*-Edge X-Ray Absorption Spectroscopy

P. ARMAND, A. IBANEZ, AND E. PHILIPPOT

Laboratoire de physicochimie des matériaux solides, URA CNRS D0407, U. M. II, Case 003, Place E. Bataillon, 34095 Montpellier Cedex 5, France

Received April 7, 1992; in revised form October 13, 1992; accepted October 15, 1992

EXAFS and XANES S *K*-edge spectra were collected at room temperature for binary GeS_x glasses ($1.5 \leq x \leq 7$) and ternary $(1 - y)GeS_2 + yAg_2S$ glasses ($0.25 \leq y \leq 0.50$). By EXAFS, only the first coordination shell was resolved. The results, for binary glasses, are consistent with the Chemical Ordered Network model: only S–Ge bonds were found for Ge-enriched glasses ($x \leq 2$) while mixed surroundings, constituted by both S–Ge and S–S bonds, exist for S-rich compositions ($x > 2$). For ternary glasses, only S–Ge bonds have been evidenced. From XANES spectra, it seems that binary S-enriched glasses are constituted by polymeric S chains cross-linked by germanium atoms. On the other hand, for ternary glasses, the XANES spectra show clearly the mixed environment of sulfur with S–Ge and S–Ag bonds. Furthermore, the sulfur surroundings seem rather similar to those of αAg_8GeS_6 for Ag_2S-enriched glasses.

I. Introduction

Germanium chalcogenide glasses present applications as memory or switching devices (*1–2*). On the other hand, thin films doped with silver are interesting materials for submicrometer lithography (*3*). Further, bulk glasses with Ag^+ cations are promising solid electrolytes (*4, 5*). Due to all these potential applications these glasses, particularly the Ge-*X* (*X* = S, Se) binary compositions, have been widely investigated for the last two decades. Although the physical properties are well known, the fundamental processes occurring in the amorphous materials are still unclear. This is mainly due to the fact that the atomic packing of these glasses is not well known.

The ternary $(1 - y)GeS_2 + yAg_2S$ glasses are highly ionically conducting and present negligible electronic conduction (*5, 6*). Furthermore, the ionic conduction phenomena of these materials are studied using different experimental techniques (*7, 8*).

In order to improve our understanding of the ionic transport processes, a structural characterization of the Ge–S and GeS_2–Ag_2S glassy systems has been undertaken by X-ray Absorption Spectroscopy (XAS). Thus, Ge *K*-edge EXAFS (Extended X-ray Absorption Fine Structures) experiments, carried out at room and low temperatures, have allowed us to characterize the first three Ge coordination spheres, thus improving our knowledge of the local and medium range order surrounding germanium atoms (*9, 10*). It has been demonstrated that Ge is fourfold coordinated in all these sulfide glasses. For GeS_x binary glasses, Ge is only surrounded by S atoms for S enriched phases ($x \geq 2$) whereas for the Ge enriched ones ($x < 2$) both Ge–S and Ge–Ge bonds exist. The existence of edge and corner sharing GeS_4 tetrahedra has been shown, demonstrating that the GeS_x glassy structures present layered clusters based on the αGeS_2 crystalline network. Furthermore, the degrees of depolymerization of corner and edge sharing tetrahedra in the glasses have been estimated from αGeS_2 crystal struc-

0022-4596/93 $5.00

ture. When the atomic composition deviates from GeS_2 stoichiometry, the depolymerization of GeS_4 clustering increases significantly leading to a structural distortion in the intermediate range order. The Ag_2S addition to glassy (g)GeS_2 induces an important increase of the depolymerization of edge and corner sharing tetrahedra leading to a distortion of the local (GeS_4 units) and of the Medium Range Order (MRO).

In addition, a Ag *K*-edge EXAFS study has been made at different temperatures (*11*). These experiments show that the silver, in these glasses, is surrounded by three sulfur atoms (Ag-S: 2.50 Å) in very distorted sites. These sites, for Ag_2S enriched glassy compositions, seem closer to those existing in the αAg_8GeS_6 crystal structure (*12*) phase than to those in the low temperature α-monoclinic form of Ag_2S, named acanthite (*13*).

To complete this structural characterization, a sulfur *K*-edge XAS analysis has been undertaken at room temperature. We report in this paper EXAFS and XANES (X-ray Absorption Near Edge Structure) results obtained for GeS_x binary blasses and for $(1 - y)GeS_2 + yAg_2S$ ternary glasses.

II. Experimental Considerations

All the syntheses were made in silica ampoules sealed under high vacuum. Bulk chalcogenide glasses were obtained by typical quenching in water (*5*). The high temperature form, αGeS_2, was synthesized from g-GeS_2 recrystallized at 700°C for an entire week. The αAg_2S phase was prepared from $AgNO_3$ and $Na_2S \cdot 9H_2O$ in a water solution and αAg_8GeS_6 was obtained from αAg_2S and g-GeS_2 compounds at 1000°C during 1 week. The different forms of sulfur were commercial chemicals: ALDRICH gold label quality for crystallized α sulfur (S_8 rings) and the polymerized ω sulfur ($[S]_n$ chains) synthesized by "OMEGA SOUFRE" company and labelled as "CROSOR D20." This ωS was dispersed, just before the XAS experiments, in CS_2 solvent in order to dissolve an eventual αS proportion. The crystalline quality or the glassy state was checked by X-ray diffraction. The atomic compositions of the glasses were measured by energy dispersive X-ray analysis.

Low energy XAS experiments, such as the S *K*-edge one (2472 eV), need very careful sample preparation to register good quality spectra. Each bulk compound was ground and sieved to obtain a homogeneous granulometry powder (5 μm). These powdered samples were then dispersed in absolute ethanol before being settled on a micropore membrane to obtain a sample deposit as homogeneous as possible. The sample concentration around 1.85 mg/cm^2 was calculated to record absorption spectra with edge step $\Delta\mu x$ of 0.5 to 0.7.

The S *K*-edge XAS spectra were registered at room temperature, on the D44 beam line of the DCI storage ring at LURE (Orsay), under vacuum to avoid important X-ray absorption by the air at these energies. The DCI storage ring was operating at 1.85 GeV with a 250-mA beam current. Data were collected in the transmission mode using two ionization chambers filled with a He–Ne mixed gas. The monochromatization was made by a double Si (111) crystal monochromator and the harmonic energies were rejected using a grazing incidence mirror (*14*). The energy calibration was recurrently checked, particularly for XANES spectra, using αS as reference (2472 eV). The energy steps and the counting time, which could be varied to satisfy the experimental requirements, were usually set at 0.1 eV and 2 sec for XANES experiments and at 1 eV and 2 sec for EXAFS spectra. The energy resolution was around 0.8 eV and several scans were necessary for each sample to improve the ratio of signal to noise.

III. XAS Data Analysis

The typical EXAFS treatment has been fully described elsewhere (*15*) and the computer programs used were adapted to a Macintosh computer by A. Michalowicz (*16*).

Background absorption was extrapolated above the threshold energy E_0 (the energy's zero point E_0 is taken at the inflection point of the absorption edge) by the Lengeler–Eisenberger analytical method (*17*) and removed from the experimental absorption coefficient signal, $\mu(E)$. The atomic absorption, $\mu_0(E)$, was approximated by a sixth degree polynomial function. The normalized EXAFS oscillations $\chi(k) = [\mu(k) - \mu_0(k)]/\mu_0(k)$ with $k(\text{Å}^{-1}) = [2m/\hbar^2 \cdot (E - E_0)]^{1/2}$ can be expressed on single scattering, plane wave, and harmonic approximations by

$$\chi(k) = -\sum_i \left[\frac{N_i \cdot F_i(\pi, k)}{k \cdot R_i^2}\right] \cdot \exp\left(\frac{-2R_i}{\lambda}\right) \cdot \exp(-2k^2\sigma_i^2) \cdot \sin(2kR_i + \Phi_i(k)),$$

where N_i is the number of scattering atoms of type i which are at an average interatomic distance R_i from the central atom, $F_i(\pi, k)$ is the backscattering amplitude, and λ is the mean free path of the photoelectron. The Debye–Waller factor σ takes into account both the static structural disorder and the atomic thermal motion and $\Phi_i(k)$ is the total phase shift of the photoelectron including the central and the backscattering atom phase shifts.

The $\chi(k)$ EXAFS oscillations were k^2 weighted and Fourier transformed (F.T.) through a Kaiser window between $k = 2$ and 12 Å^{-1}. The simulations of the Fourier filtered experimental signals have been performed using a mean-square fitting procedure, and the backscattered phases and amplitudes used were those calculated by McKale *et al.* (*18*).

Thus, these adjustments have led to the determination of the structural parameters R, N, and σ. Different treatments carried out on independent spectra of each sample have allowed us to estimate the statistical errors made on each parameter.

To compare the different XANES spectra between themselves, first the absorption background subtraction has been made by a Victoreen law, then the spectra were normalized by taking an energy point as close as possible to the atomic absorption $\mu_0(E)$ around 80 eV above the absorption edge (*19*).

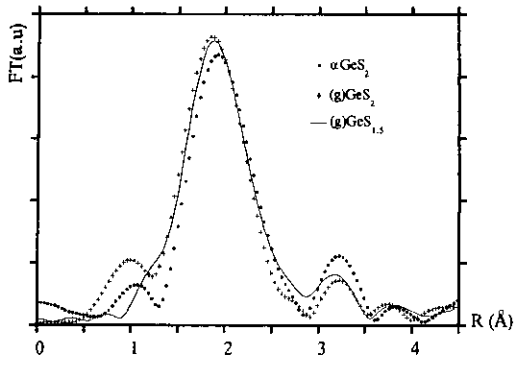

FIG. 1. F.T. magnitudes, uncorrected for phase shift, of g-$GeS_{1.5}$ and g-GeS_2, compared to that of αGeS_2.

IV. Results

IV.1. EXAFS Results

The k range restriction at $k_{max} = 12$ Å^{-1}, due to an important increase of the noise at higher energies, induces truncation effects by Fourier transforming. This is illustrated in Figs. 1 and 2 where the F.T. moduli, uncorrected for phase shifts, of GeS_x glasses, αGeS_2 and αS, are presented. In all cases, only the first sulfur coordination shell has been revealed.

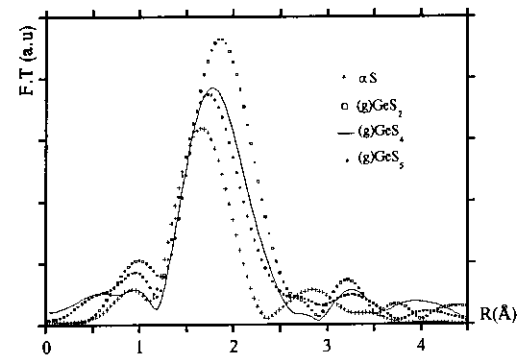

FIG. 2. $k^2\chi(k)$ Fourier transform moduli, without phase correction, obtained for S-enriched GeS_x glasses ($x \geq 2$) compared with the modulus for αS.

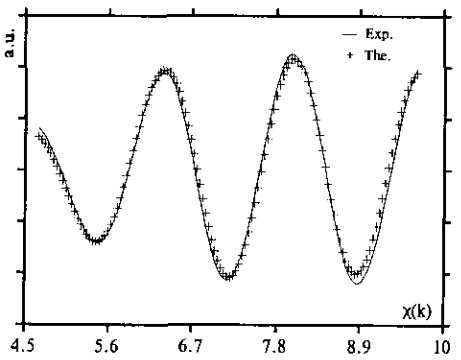

FIG. 3. Simulation of $k^2\chi(k)$ experimental signal for the g-GeS_2 phase.

IV.1.a. Germanium enriched GeS_x glasses ($x \leq 2$). Fourier transformed magnitudes of g-$GeS_{1.5}$ and g-GeS_2, compared to the αGeS_2 one in Fig. 1, show that the sulfur first coordination sphere is very similar for all these phases. However, the F.T. magnitude peak of the glasses is slightly shifted towards lower distances R and presents a slightly higher intensity compared to the αGeS_2 one (Fig. 1). The first simulations of the Fourier filtered EXAFS signals were made by using experimental backscattered phases and amplitudes extracted from αGeS_2 spectra. These adjustments lead to incorrect values of the structural parameters with coordination numbers of sulfur too weak, around 1.5, and Debye–Waller factors $\Delta\sigma = \sigma_{glass} - \sigma_{\alpha GeS_2}$ remaining always equal to zero. Furthermore, the S–Ge bond lengths obtained (2.18 Å) are too short as compared to the Ge K-edge EXAFS results (2.22 Å) (*9*, *10*). Thus, a new series of simulations of the EXAFS signals has been carried out using the theoretical backscattered phases and amplitudes calculated by McKale *et al.* (*18*).

The Fourier filtered experimental signals of g-$GeS_{1.5}$ and g-GeS_2 have first been well simulated (Fig. 3) by fitting simultaneously all the structural parameters, N, R, $\Delta\sigma$, and ΔE_0, in a one shell model (sulfur surrounded only by germanium atoms). Thus, this quantitative analysis seems to show that each sulfur atom is surrounded only by two germanium atoms at an average distance of 2.21 ± 0.01 Å which is in accordance with the previous Ge K-edge EXAFS results (*9*, *10*). Furthermore, the weak values obtained for the Debye–Waller factor ($\sigma \sim 0.005$ Å) show the nondistorted surroundings of sulfur atoms in the glasses. These adjustments of the structural parameter have demonstrated that the higher peak intensity of F.T. magnitude, registered for the glasses compared to the αGeS_2 one (Fig. 1), is due to Debye–Waller values, σ, lower than for αGeS_2. Thus, it seems that the local surroundings of sulfur in the glass are less distorted than in the αGeS_2 crystalline network. This phenomenon, already registered for these materials around germanium atoms by a Ge K-edge EXAFS study (*9*), can be explained by structural constraints due to long range order in the αGeS_2 crystal structure. Thus αGeS_2 cannot be a good EXAFS reference in this study.

On the other hand, to confirm the absence of S–S homopolar bonds in this glassy range ($x \leq 2$), the simulations of the EXAFS oscillations have then been carried out in a two shell model including S–Ge and S–S bonds. In fact, the number of independent points for the inverse F.T. signal $N_{pts} = 2\,\Delta k \cdot \Delta R/\pi = 9$ (Δk (Å^{-1}) and ΔR (Å) are the windows used respectively in energy and distance range for the Fourier filtering procedure) allows us to adjust eight parameters at the same time. The results coming out of these new adjustments of g-$GeS_{1.5}$ and g-GeS_2 signals, presented in Table I, corroborate the twofold coordination of sulfur with germanium without S–S homopolar bonds. Furthermore, the Debye–Waller values are very low, indicating that the distribution of bond lengths is very narrow and that the sulfur thermal motion is very weak.

On the other hand, the F.T. moduli seem to present a second coordination shell around 3.1 Å (Fig. 1) which could correspond, taking the phase shifts into account, to S · · · S distances (3.6 Å) existing in the αGeS_2 structure. However, the F.T. trunca-

TABLE I

S *K*-EDGE EXAFS RESULTS FOR BINARY GeS_x GLASSES ($1.5 \leq x \leq 5$)

		N	R (Å)	$\Delta\sigma$ (Å)	E_0 (eV)	Reliability factor
$GeS_{1.5}$	S–Ge	2.0(2)	2.22(2)	0.005	−1.8	5×10^{-2}
	S–S	0.01	2.05(1)	0.002		
GeS_2	S–Ge	2.0(1)	2.21(1)	0.004	−1.2	3×10^{-2}
	S–S	0.01	2.05(1)	0.001		
GeS_3	S–Ge	1.8(1)	2.21(1)	0.005	−3.7	2×10^{-2}
	S–S	0.2(1)	2.05(1)	0.002		
GeS_4	S–Ge	1.7(1)	2.20(2)	0.005	−5.8	1×10^{-2}
	S–S	0.3(1)	2.06(1)	0.002		
GeS_5	S–Ge	1.4(2)	2.20(2)	0.004	−5.7	3×10^{-2}
	S–S	0.6(2)	2.05(1)	0.002		

tion effects forbid any EXAFS characterization of this second shell.

IV.1.b. Sulfur enriched GeS_x glasses ($x > 2$). F.T. magnitudes uncorrected for phase shifts of sulfur-enriched glasses are compared to the αS one in Fig. 2. A gradual decrease of the F.T. peak intensity and a progressive shift of its position towards lower distances are registered when the sulfur proportion increases in the glass. To simulate correctly the F.T. filtered EXAFS signals of these glasses, a two shell model was necessary. The adjustment results, Table I, show mixed surroundings for S rich compositions constituted by both S–Ge (2.21 ± 0.01 Å) and S–S (2.05 ± 0.01 Å) bonds. Furthermore, the S–S bond proportion increases logically with the sulfur content in the glass but we obtain only a qualitative agreement in the trend. This is certainly due to the too narrow k-range (2–12 $Å^{-1}$) used and to the weak signal-to-noise ratios of normalized EXAFS oscillations extracted. As for Ge enriched glasses, the Debye–Waller values remain very weak.

IV.1.c. Ternary (1-y) GeS_2 + y Ag_2S *glasses.* The X-ray absorption of these ternary glasses increases drastically with the addition of silver at this energy range around S *K*-edge. Thus, in the transmission mode it is very difficult to record EXAFS spectra with a good ratio of signal to noise. To obtain correct statistics, we have accumulated several scans for the ternary $0.75GeS_2 + 0.25Ag_2S$ sample. The F.T. magnitude of this glass, Fig. 4, presents only one first coordination peak which is very similar to those registered for GeS_x binary compounds. After this, the simulation of the sulfur surroundings needs only one germanium coordination shell. Indeed, the fitted structural parameters obtained for the first neighboring sulfur in $0.75GeS_2 + 0.25Ag_2S$ glass are 1.7 Ge atoms at 2.21 Å with σ = 0.04 Å. The higher Debye–Waller value obtained for this ternary glass shows that the S sites are more distorted in this case than in the binary glasses. The S–Ag bonds, already characterized by Ag *K*-edge XAS study, have not been revealed here. This is certainly due to the very high values of the Debye–Waller factors for the silver subshell, as previously found by the Ag *K*-edge EXAFS results (*11*). In fact, the high mobility of silver cations in the glassy network must attenuate the major part of the EXAFS contributions of the silver subshell. Furthermore, due to problems of noise, a narrow k range (2–11 $Å^{-1}$) has been used. This procedure has not allowed us to characterize silver atoms whose backscattering contributions intervene at k values higher than those of sulfur atoms.

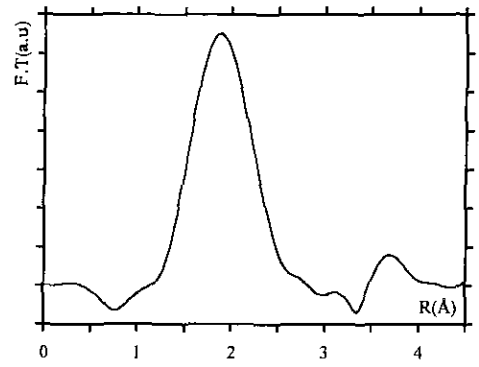

FIG. 4. $k^2\chi(k)$ F.T. magnitude, uncorrected for phase shift, of $0.75GeS_2 + 0.25Ag_2S$ ternary glass.

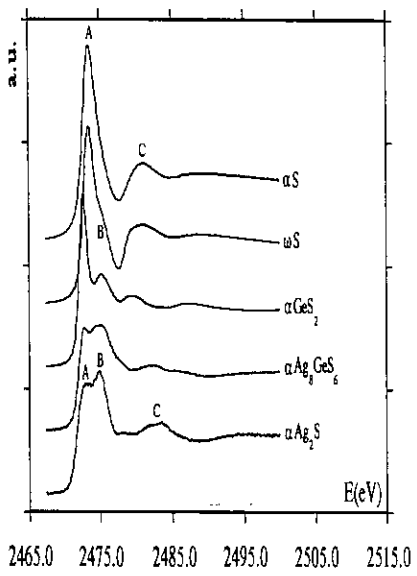

FIG. 5. XANES spectra obtained for crystallized phases.

IV.2. XANES Results

The XANES spectra registered for well known phases of the Ag–Ge–S system are presented first. Afterward, these reference results are discussed to characterize the structure of germanium chalcogenide glasses.

Thus, XANES spectra of αGeS_2 (*20*), native sulfur αS (*21*), polymerized ωS (*22, 23*), αAg_8GeS_6 (*12*), and αAg_2S (*13*) phases have been collected. The different spectra obtained are shown in Fig. 5. They exhibit several XANES resonances labeled, from the edge, A, B, and C. Their energy positions (peak maximum) and the position of the absorption threshold E_0 taken at the maximum of the derivative absorption curve are given in Table II. We have then tried to explain the origin of these resonances. For that, we have taken into account the atomic nature of the different elements involved in these phases and of several previous XANES works made at the sulfur *K*-edge on rather comparable materials (*24–27*). The features of S *K*-edge XANES spectra in the first 10 eV above the edge (threshold region) are mainly induced by the electronic density of the empty states. The dipolar selecting rule is predominant ($\Delta l = \pm 1$) and the first empty states are governed by the degree and the nature of the chemical bonds between sulfur and its first neighboring atoms in the solid state.

In αS and ωS structures, each sulfur atom forms two pure covalent bonds S–S (2.05 Å) mainly due to $3p$(S)–$3p$(S) overlaps, the electric charge on sulfur is zero, and its electronic configuration is [Ne] $3s^2 3p^4$. In the case of αGeS_2, sulfur has two heteropolar S–Ge bonds (2.21 Å) mainly constituted from $3p$(S)–$4sp^3$(Ge) hybridizations with a weakly ionic character (the difference in Pauling's electronegativity between sulfur and germanium is 0.7) leading to a weak negative electric charge, $-\delta$, on sulfur ([Ne] $3s^2 3p^{4+\delta}$).

For the αAg_8GeS_6 and αAg_2S phases, the ionicity character increases with the S–Ag bond proportion, thus inducing an increase of δ on sulfur (i.e., an increase of the $3p$ electron number). Nevertheless, in these two compounds each silver atom presents two or three sulfur neighboring atoms between 2.5 Å and 2.6 Å (*12, 13*). These bond lengths, near to the sum of covalent radii ($\Sigma_{covalent}$ = 2.55 Å and Σ_{ionic} = 3.10 Å), the low Ag coordination, and the weak difference in Pauling's electronegativity between sulfur and silver (0.6) suggest that the shortest S–Ag bonds have a nonnegligible covalent character as has been suggested by

TABLE II

ENERGIES OF THE RESONANCES AND OF THE ABSORPTION THRESHOLDS, E_0 OF THE CRYSTALLINE PHASES

	E_0 (eV)	A (eV)	B (eV)	C (eV)
αS	2472.6	2473.4	—	2480.9
ωS	2472.7	2473.3	2475.3	2480.8
αGeS_2	2472.0	2472.6	2475.0	2479.6
αAg_8GeS_6	2471.8	2472.7	2474.9	2482.1
αAg_2S	2471.7	2473.2	2474.9	2483.5

other authors for the corresponding selenide glasses (*28–30*).

Thus, the white line, A, can be assigned to electron transitions from $1s$ initial states to the first empty states involving the $3p$(S) atomic orbitals in the solid state. These electron transitions are generally labeled, for convenience, $1s \rightarrow 3p$ in the atomic picture (*24–27*). The second peak, B, around 5–6 eV above the Fermi level, would be partly due to empty states in the conduction band of the solids involving higher p symmetry levels of sulfur atoms. For convenience, we have labeled this transition $1s \rightarrow$ "$4p$".

Reviewing the spectra from the two sulfur forms αS and ωS, then from αGeS_2, and finally from αAg_8GeS_6 and αAg_2S, we note a shift of the absorption threshold to lower energies (Table II), an intensity decrease of the white line A, and an increase of the second peak, B, intensity (Fig. 5). Thus, the evolution of these spectra seems directly connected to the increase of the partial ionic character of the bonds involved by sulfur atoms. In fact, the transition probability given by the Fermi law is directly proportional to the density of empty states. When the sulfur electric charge increases, δ, (augmentation of the chemical bond ionicity of sulfur, S–Ge, S–Ag) the $3p$ level fills up inducing a decrease of the $1s \rightarrow 3p$ transition probability while the $1s \rightarrow$ "$4p$" one is favoured. These electron transition phenomena explain perfectly the intensity evolutions registered in Fig. 5 for the first two peaks, A and B.

On the other hand, the absorption coefficients depend on the transition dipole matrix M_{ij}. In a previous study (*31*), it has been shown that an increase of the valence electron density (increase of $3p$ density on sulfur due to ionicity in our case) increases the screening effect of the nuclear potential of the central element leading to an augmentation of M_{ij}. This screening effect, which operates in the same way on the intensity of the white line, A, as that of the density of empty states, however, seems to be a less important phenomena. But this screening effect would also explain the energy shifts of the absorption threshold, E_0 (Table II). Indeed, this effect, easily registered in photoemission spectroscopy (*32*), leads to an energy reduction of the core electron levels inducing typical chemical shifts. Nevertheless, these chemical shifts of the core levels $1s$(S) are only a partial explanation because in XANES spectra the measured energies depend also on the final state of the electron.

Although the XANES spectra are strongly influenced in the edge region by the density of unoccupied states, long and short range multiple scattering provides an overriding modulation which becomes predominant above the continuum threshold, E_c (ionization potential of the core level). The multiple scattering range is directly connected to the mean free path, λ, of the photoelectron which depends on its energy ($\lambda \sim 20$ Å for E $\sim$ 10 eV, $\lambda \sim 8$ Å for E $\sim$ 20 eV) (*33, 34*).

Thus the origin of the C resonances, Fig. 5, is difficult to establish because they are certainly close to E_c. It certainly corresponds to a maximum of the solid state density which is due more to the sulfur surrounding geometry (multiple-scattering resonance) than to the electronic properties.

The XANES spectra of the two sulfur forms αS and ωS are very similar. However, in the ωS case, we can note a shoulder feature, B, just after the white line, A, which does not appear for the αS form, Fig. 5. This small difference is more distinguishable by the absorption derivative curves, Fig. 6. At this weak energy, the mean free path of the photoelectron allows it to probe the M.R.O. of these phases involving multiple scattering effects (*34*). Now, if the structures of elemental sulfur present identical Short Range Order (S.R.O.) around S atoms, they present different M.R.O.: S_8 rings for the αS structure and $[S]_n$ screws for the ωS one. Thus, the existence or not of a white line shoulder around 5 eV above E_0 could be a fingerprint of the M.R.O.

I.V.2.a. Germanium enriched GeS_x binary glasses. The XANES spectra of

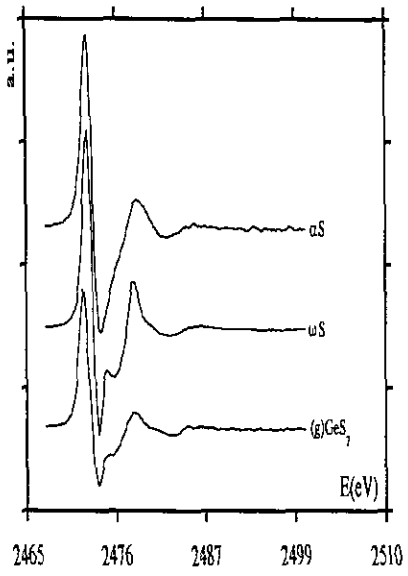

FIG. 6. αS and ωS derivative XANES curves, compared to that of the binary glass GeS_7.

αGeS_2, g-GeS_2, g-$GeS_{1.7}$, and g-$GeS_{1.5}$ are shown in Fig. 7. All these spectra are very similar in agreement with the identical S local surroundings demonstrated by EXAFS. However, we note between αGeS_2 and the glassy phases a broadening and an intensity reduction of the different peaks due to the typical disorder effects. The high similitude between the αGeS_2 and g-GeS_2 spectra confirms that the GeS_2 glassy structure around sulfur is based on the crystallized one at the short and medium range order. This is consistent with the previous results obtained around germanium (*10*).

When the glassy composition is enriched in germanium, the intensity of the resonance B decreases to leave only a shoulder feature for g-$GeS_{1.5}$, Fig. 7. This evolution is certainly due to M.R.O. changes induced by the formation of Ge–Ge homopolar bonds.

IV.2.b. Sulfur enriched binary glasses. The XANES spectra of GeS_x ($x \geq 2$) glassy phases are compared to the αS and ωS ones in Fig. 8. The EXAFS study has shown that there are S–S homopolar bonds in GeS_x sulfur-enriched glasses ($x > 2$). The $1s \rightarrow 3p$ electron transitions corresponding to the pure covalent S–S bonds appear at higher energies than those of S–Ge bonds as already explained above. Thus, the existence of both S–S and S–Ge bonds for the S-enriched glasses leads to a broadening of the white line, A, and to a lowering of its intensity, Fig. 8 and Table III.

On the other hand, the intensity of the B resonance gradually decreases as the sulfur proportion increases in the glasses, to become only a shoulder for the very enriched sulfur compositions (GeS_7), Fig. 8. This might be partly explained by a lessening of the $1s \rightarrow$ "$4p$" transition probability for a high proportion of pure S–S covalent bonds. Nevertheless, this structure B is also strongly influenced by M.R.O. modifications taken into account by the multiple scattering effects. Furthermore, both the intensity and the energy of the C resonance increase for higher sulfur concentrations, Table III. Thus, the spectra of very enriched sulfur glasses present a strong resemblance to the ωS one, Fig. 8 and Table III, while the αS spectrum does not present a shoulder

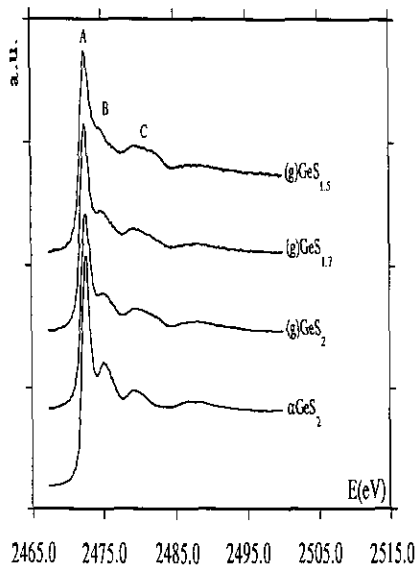

FIG. 7. XANES curves obtained for Ge-enriched GeS_x glasses ($x \leq 2$) and αGeS_2.

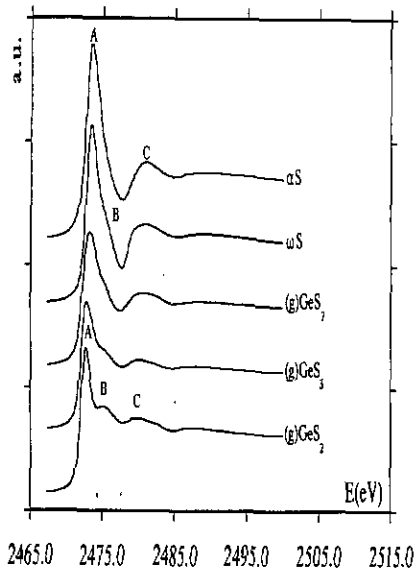

FIG. 8. XANES spectra of S-enriched GeS_x glasses ($x \geq 2$) compared with those of both crystalline sulfur forms α and ω.

structure B certainly resulting, as we have seen, in a different M.R.O. The difference between S-enriched glasses and ωS spectra and that of αS is well illustrated by the derivative curves, Fig. 6. This seems to indicate that the M.R.O. of high sulfur content glasses is closer to the polymerized ωS M.R.O. than to the other M.R.O. constituted by S_8 rings in αS.

IV.2.c. $(1-y)\ GeS_2 + yAg_2S$ ternary glasses. The addition of the glassy network modifier Ag_2S to the GeS_2 glass former gives

TABLE III

ENERGIES OF THE RESONANCES AND OF THE ABSORPTION THRESHOLDS, E_0, OF S-ENRICHED GLASSES, ωS AND αS

	E_0 (eV)	A (eV)	B (eV)	C (eV)
g-GeS_2	2472.0	2472.6	2475.0	2479.6
g-GeS_3	2472.1	2472.8	2475.4	2480.0
g-GeS_5	2472.1	2473.1	2475.3	2480.4
g-GeS_7	2472.1	2473.2	2475.3	2480.7
ωS	2472.7	2473.3	2475.3	2480.8
αS	2472.6	2473.4	—	2480.9

TABLE IV

ENERGIES OF THE RESONANCES AND OF THE ABSORPTION THRESHOLDS, E_0, OF TERNARY GLASSES AND CRYSTALLINE COMPOUNDS

	E_0 (eV)	A (eV)	B (eV)	C (eV)
$y = 0.25$	2471.8	2472.5	2474.9	2478.9
$y = 0.40$	2471.8	2472.5	2474.8	2479.3
$y = 0.50$	2471.8	2472.7	2474.8	2479.9
α-Ag_8GeS_6	2471.8	2472.7	2474.9	2482.1
αAg_2S	2471.7	2473.2	2474.9	2483.5

rise for XANES spectra to a slight reduction of the threshold energy, E_0 (Table IV), and to a lowering of the white line A intensity. Moreover, the resonance B intensity increases significantly, Fig. 9. These evolutions already encountered in Fig. 5 for crystalline compounds are due, as shown above, to an increase of the partial ionicity of the chemical bond involved by sulfur atoms. Thus, the evolution of these spectra can be connected to the existence of S–Ag bonds in ternary glasses as already found in the silver *K*-edge EXAFS study (*11*).

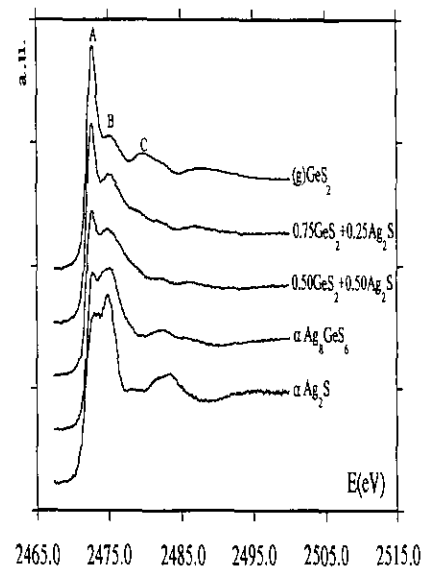

FIG. 9. Comparison of αAg_2S, αAg_8GeS_6, and g-GeS_2 XANES curves with those of $(1-y)GeS_2 + yAg_2S$ ($y = 0.25$ and 0.50) ternary glasses.

Furthermore, the intensity of the C peak decreases for ternary glasses, compared to g-GeS_2, and its energy position moves toward that registered for α-Ag_8GeS_6, Table IV. Thus, for the highest Ag_2S concentrations, the glasses present XANES spectra closer to the αAg_8GeS_6 one than to the αAg_2S spectrum, Fig. 9 and Table IV.

V. Structural Conclusions

The sulfur *K*-edge XAS experiments have allowed us to complete our structural approach of germanium chalcogenide glasses. The sulfur local surroundings have been determined by EXAFS as already made for germanium and silver atoms. On the other hand, the XANES spectra of the glasses have been compared to those of known phases used as the standards. A qualitative characterization of the glassy structure confirming the S.R.O results and giving some M.R.O. indications has been made in this way.

Thus, we have demonstrated that the sulfur atom is surrounded by 2 Ge atoms (S–Ge : 2.21 Å) for Ge enriched GeS_x glasses ($x \leq 2$), while a mixed S environment with S–Ge and S–S (2.05 Å) appears only for S enriched compositions ($x > 2$). These results are in perfect agreement with the previous ones (*9*), obtained at the Ge *K*-edge, showing the existence of Ge–Ge homopolar bonds for g-GeS_x when $x < 2$. This confirms that the formation of these binary glasses is controlled by a chemically ordered process (chemically ordered network model (*35*)) and is consistent with the maximum of glass transition temperature T_g registered for GeS_2 stoichiometric glass (*36*).

Furthermore, the high similarity between the S *K*-edge XANES spectra of g-GeS_2 and αGeS_2 is also consistent with our Ge *K*-edge study. Indeed, this XANES similarity seems to confirm that the glassy structure is based on the layered crystalline network, with GeS_4 tetrahedral units clustered by edges and corners, in agreement with the "outrigger raft" model (*37, 38*) and with other recent studies (*39*). Nevertheless, the "outrigger raft" model suggests for g-GeX_2 (X = S,Se) the formation of X–X bonds at the boundaries of the layered clusters (raft). These homopolar bonds between chalcogen atoms have not been revealed by our EXAFS study. Thus, the g-GeX_2 structure is certainly constituted by "layered" clusters with edge and corner sharing GeX_4 tetrahedra distorted in the glassy state, leading to a three-dimensional structure. This "distorted crystalline network" hypothesis is an intermediate model between the "outrigger raft" and the "continuous random network" ones.

On the other hand, the XANES spectra of S-enriched glasses are consistent with the mixed surroundings of sulfur. They seem to indicate, too, that the M.R.O. of high sulfur content glasses is closer to the polymerized M.R.O. of ωS than to that of αS with S_8 rings. Thus, the augmentation of S–S bond proportion would lead to the formation of polymeric S chains cross-linked with Ge, rather than of rings. This is consistent with our recent Anomalous Wide Angle X-ray Scattering (AWAXS) experiments made on selenide glasses (g-$GeSe_3$ and g-$GeSe_5$) (*40*) and also with the "cross-linked chains model" (*41*).

For $(1 - y)GeS_2 + yAg_2S$ ternary glasses, the S *K*-edge EXAFS characterization of S–Ag bonds has failed. Nevertheless, the XANES spectra clearly reveal mixed S surroundings with S–Ge and S–Ag bonds as already found in the Ag *K*-edge XAS study. In addition, it seems that the glasses with important silver concentrations present sulfur environments more similar to those encountered in the αAg_8GeS_6 crystalline structure, with a coordination number above two. This similarity is consistent with the silver *K*-edge study (*11*) and with other works using scattering techniques (*42*).

Acknowledgments

The authors are grateful to H. Dexpert for stimulating collaborations and helpful discussions. We also express

appreciation to D. Bazin for helpful assistance in data acquisition performance.

References

1. B. T. Kolomiets, *Phys. Status Solidi* **7,** 359 (1964).
2. S. R. Ovshinsky, *Phys. Rev. Lett.* **21,** 1450 (1968).
3. D. A. Doane and A. Heller, Eds., "Proc. Symp. Inorganic Resist Systems," Electrochemical Soc. (1982).
4. E. Robinel, B. Carette, and M. Ribes, *J. Non-Cryst. Solids* **57,** 49 (1983).
5. J. L. Souquet, E. Robinel, B. Barrau, and M. Ribes, *Solid State Ionics* **3–4,** 317 (1981).
6. E. Robinel, A. Kone, M. J. Duclot, and J. L. Souquet, *J. Non-Cryst. Solids* **57,** 59 (1983).
7. J. Roos, D. Brinkmann, M. Mali, A. Pradel, and M. Ribes, *Solid State Ionics* **28–30,** 710 (1988).
8. A. P. Owens, A. Pradel, M. Ribes, and S. R. Elliott, *J. Non-Cryst. Solids* **131–133,** 1104 (1991).
9. A. Ibanez, E. Philippot, S. Benazeth, and H. Dexpert, *J. Non-Cryst. Solids* **127,** 25 (1991).
10. P. Armand, A. Ibanez, H. Dexpert, and E. Philippot, *J. Non-Cryst. Solids* **139,** 137 (1992).
11. A. Ibanez, P. Armand, H. Dexpert, and E. Philippot, *Solid State Ionics* **59,** 157 (1993).
12. G. Eulenberger, *Monatsh. Chem.* **108,** 901 (1977).
13. R. Sadanaga and S. Sueno, *Mineral. J.* **5,** 124 (1967).
14. P. Sainctavit, J. Petiau, A. Manceau, R. Rivallant, M. Belakhovsky, and G. Renaud, *Nucl. Instrum. Methods Phys. Res.* **A273,** 423 (1988).
15. B. K. Teo and P. A. Lee, *J. Am. Chem. Soc.* **101,** 2815 (1979).
16. A. Michalowicz, *in* "Logiciels pour la chimie" (Société Française de Chimie, Ed.), p. 102, Paris (1991).
17. B. Lengeler and P. Eisenberger, *Phys. Rev. B* **21,** 4507 (1980).
18. A. C. McKale, B. W. Veal, A. P. Paulilkas, S. K. Chan, and G. S. Knapp, *J. Am. Chem. Soc.* **110,** 3763 (1988).
19. A. Michalowicz, and V. Noinville, *in* "Logiciels pour la chimie" (Société Française de Chimie, Ed.), p. 116, Paris (1991).
20. G. Dittmar and H. Schafer, *Acta Crystallogr. Sect. B* **31,** 2060 (1975).
21. A. Caron and J. Donohue, *Acta Crystallogr.* **14,** 548 (1961).
22. F. Tuinstra, *Acta Crystallogr.* **20,** 341 (1966).
23. M. D. Lind and S. Geller, *J. Chem. Phys.* **51,** 348 (1969).
24. P. Sainctavit, PhD. thesis, Université Paris VII (1989).
25. P. Sainctavit, J. Petiau, A. M. Flank, J. Ringeisen, and D. G. Montague, *Physica B* **158,** 623 (1989).
26. M. Kitamura, C. Sugiura, and S. Muramatsu, *Solid State Commun.* **67,** 313 (1988).
27. J. Olivier-Fourcade, A. Ibanez, J. C. Jumas, H. Dexpert, C. Blancard, J. M. Esteva, and R. C. Karnatak, *Eur. J. Solid State Inorg. Chem.* **28,** 409 (1991).
28. L. C. Bourne, S. C. Rowland, and A. Bienenstock, *J. Phys. C* 4(10), 951 (1981).
29. R. J. Dejus, S. Susman, K. J. Volin, D. G. Montague, and D. L. Price, *J. Non-Cryst. Solids* **143,** 162 (1992).
30. J. M. Oldale, J. Rennie, and S. R. Elliot, *Thin Solid Films* **164.** 467 (1988).
31. K. J. Rao, J. Wong, and M. W. Shafer, *J. Solid State Chem.* **55,** 110 (1984).
32. M. Cardona and L. Ley, Eds., "Photoemission in Solids I," p. 60, Springer-Verlag, Berlin/New York (1978).
33. B. K. Teo, "EXAFS: Basic Principles and Data Analysis," p. 92, Springer-Verlag, Berlin/New York (1986).
34. A. Bianconi, *in* "X-Ray Absorption" (D. C. Koningsberger and R. Prins, Eds.), p. 573, Wiley–Interscience, New York (1988).
35. G. Lucovsky, F. L. Galeener, R. C. Keeser, R. H. Geils, and H. Six, *Phys. Rev. B* **10,** 5134 (1974).
36. J. Malek, *J. Non-Cryst. Solids* **107,** 323 (1989).
37. N. Kumagai, J. Shirafuji, and Y. Inuishi, *J. Phys. Soc. Jpn.* **42,** 1261 (1977).
38. J. E. Griffiths, J. C. Philips, G. P. Espinosa, J. P. Remeika, and P. M. Bridenbaugh, *Phys. Status Solidi B* **122,** K11 (1984).
39. J. Heo and J. D. Mackenzie, *J. Non-Cryst. Solids* **113,** 1 (1989).
40. P. Armand, A. Ibanez, E. Philippot, Q. Ma, and D. Raoux, *in* "Proc. 5th Int. Conf. Structure of Non-crystalline Materials, Sendai, Japan, Sept. 1991," *J. Non-Cryst. Solids* **150,** 371 (1992).
41. J. P. de Neufville, *J. Non-Cryst. Solids* **8–10,** 85 (1972).
42. R. J. Dejus, S. Susman, K. J. Volin, D. L. Price, and D. G. Montague, *J. Non-Cryst. Solids* **106,** 34 (1988).